

# Using strong electromagnetic fields to control x-ray processes

Linda Young,<sup>1</sup> Christian Buth,<sup>1,\*</sup> Robert W. Dunford,<sup>1</sup> Phay J. Ho,<sup>1</sup> Elliot P. Kanter,<sup>1</sup> Bertold Krässig,<sup>1</sup> Emily R. Peterson,<sup>1</sup> Nina Rohringer,<sup>1,†</sup> Robin Santra,<sup>1,2</sup> and Stephen H. Southworth<sup>1</sup>

<sup>1</sup>Argonne National Laboratory, Argonne, Illinois 60439, USA

<sup>2</sup>Department of Physics, University of Chicago, Chicago, Illinois 60637, USA

(Dated: September 20, 2008)

Exploration of a new ultrafast-ultraspeed frontier in atomic and molecular physics has begun. Not only is it possible to control outer-shell electron dynamics with intense ultrafast optical lasers, but now control of inner-shell processes has become possible by combining intense infrared/optical lasers with tunable sources of x-ray radiation. This marriage of strong-field laser and x-ray physics has led to the discovery of methods to control reversibly resonant x-ray absorption in atoms and molecules on ultrafast timescales. Using a strong optical dressing field, resonant x-ray absorption in atoms can be markedly suppressed, yielding an example of electromagnetically induced transparency for x rays. Resonant x-ray absorption can also be controlled in molecules using strong non-resonant, polarized laser fields to align the framework of a molecule, and therefore its unoccupied molecular orbitals to which resonant absorption occurs. At higher laser intensities, ultrafast field ionization produces an irreversible change in x-ray absorption. Finally, the advent of x-ray free electron lasers enables first exploration of non-linear x-ray processes.

## INTRODUCTION

Control of x-ray processes using intense optical lasers represents an emerging scientific frontier—one which combines x-ray physics with strong-field laser control [1]. While the past decade has produced many examples where intense lasers at optical wavelengths are used to control molecular motions [2, 3, 4, 5], extension to the control of intraatomic inner-shell processes is quite new [1, 6, 7, 8]. At first glance, it is an unusual concept to control x-ray processes using an optical or infrared radiation field since x-rays interact predominantly with inner-shell electrons, whereas longer wavelength radiation interacts with outer shell electrons. However, the inner and outer shells of atoms are coupled through resonant x-ray absorption, e.g., promotion of a *K*-shell electron to an empty outer shell orbital, as shown in Fig. 1. Because outer shell electronic structure can be perturbed (dressed) by an optical radiation field, one can exert control over resonant x-ray absorption using optical lasers. Reversible control is possible when the applied dressing field is gentle enough to significantly perturb outer-shell electronic structure, but is not intense enough to destroy (ionize) the atom.

Let us consider the optical field amplitude necessary to achieve this control, i.e., to induce outer-shell transitions at a rate comparable to inner-shell processes. If we take the simplest case, shown in Fig. 1, where absorption of an x-ray photon leads to the ejection of a *K*-shell electron, a  $1s^{-1}$  hole is created. The resulting atom, containing a  $1s^{-1}$  hole, is unstable and decays via both radiative and non-radiative (Auger) channels [9]. These inner-shell decay rates increase with atomic number; at  $Z = 10$  the lifetime of the  $1s^{-1}$  hole state is 2.4 fs (corresponding to a 0.27 eV level width via the uncertainty principle). In order to compete with the rapid inner-shell

decay, electromagnetic transitions in the outer shell must be induced at a comparable rate. The transition rate in a driven two-level system is given by the Rabi flopping frequency,  $\Omega_{12} = \mu_{12}E/\hbar$  where  $\mu_{12} = \langle 1|ez|2\rangle$  is the transition dipole matrix element between levels 1 and 2,  $E$  is the electric field amplitude. In practical units,  $E$  is related to the laser intensity via  $I[\text{W}/\text{cm}^2] = (1/2Z_0)E^2 [\text{V}/\text{cm}]$ , where  $Z_0 = \sqrt{\mu_0\epsilon_0} = 377 \text{ V}/\text{A}$  is the vacuum impedance. To estimate the laser intensity required to drive Rabi oscillations at a rate comparable to inner shell decay we use atomic units which are related to the hydrogen atom: charge,  $e = 1$ ; length = Bohr radius =  $a_0$ ; velocity = Bohr velocity  $v_0 = \alpha c$ ; electric field = field at the Bohr radius  $e/a_0^2 \sim 51 \text{ V}/\text{\AA}$ ; electric dipole moment =  $ea_0$ , time  $t_0 = a_0/v_0 \sim 0.024 \text{ fs}$ . For the hydrogen  $1s \rightarrow 2p_{1/2}$  transition,  $\mu_{12} = 1.05ea_0$ . Combining this with an electric field amplitude  $E = 1$  atomic unit, the Rabi flopping frequency will be  $\Omega_{12} = 1/t_0 = 1/0.024 \text{ fs}$ . The laser-induced rate is  $16\times$  that of the decay rate of the  $1s$  hole state in neon! ( $\Omega_{12}$  are given in angular frequency units) Therefore, if the electric field amplitude of the optical laser can be 1 atomic unit, or equivalently a laser intensity of  $3.5 \times 10^{16} \text{ W}/\text{cm}^2$ , outer-shell transition rates can exceed inner-shell decay rates.

This intensity can now be achieved with routinely available modern lasers [10, 11]. The key development of chirped pulse amplification [12] permits increased output energies from ultrashort lasers without damage to amplifying media. Focusing a standard amplified Ti:sapphire laser (800 nm, 3 mJ, 40 fs, 1 kHz) to  $15 \mu\text{m}$  produces  $I \sim 3.5 \times 10^{16} \text{ W}/\text{cm}^2$ . Ti:sapphire lasers are very versatile; the wide bandwidth allows one to stretch the pulsewidth from tens of femtoseconds to hundreds of picoseconds, and permitting the study of atoms and molecules exposed to a wide range of electromagnetic field strengths.

After the strong optical laser field, the next ingredient

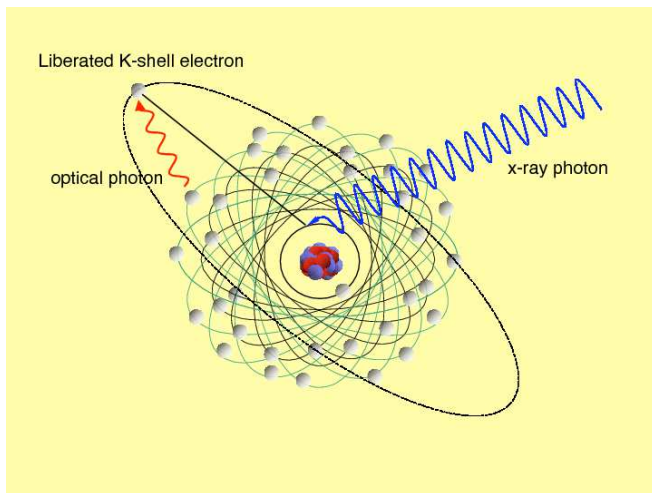


FIG. 1: (Color online) X-ray absorption promotes a  $1s$  electron to an empty outer shell orbital. Optical radiation induces transitions between outer shell orbitals. Inner and outer shells are coupled through resonant x-ray absorption.

needed to study control of ultrafast inner-shell processes is a tunable x-ray source. Synchrotrons provide a convenient source of pulsed, tunable, polarized radiation from 10 eV to 100,000 eV. This range covers inner shell edges of all elements. In Fig. 2 the three dominant photoprocesses, photoabsorption, elastic (Rayleigh) scattering and inelastic (Compton) scattering are shown for the bromine atom. Photoabsorption cross sections greatly exceed scattering cross sections over energy ranges from below to far above the respective  $K$  edges of each atom. In order to probe atoms and molecules subjected to strong pulsed optical fields, a short x-ray pulse is helpful. A typical x-ray pulse length is 100 ps at the Argonne Advanced Photon Source. For a 100 ps x-ray pulse duration, one can probe atoms and molecules subjected to  $10^{12}$  W/cm<sup>2</sup> with millijoule laser pulse energies focused to tens of microns. Shorter pulse lengths,  $\sim 100$  fs, at synchrotron sources are currently available using laser slicing techniques conceived by Zholents and Zolotarev [13] and put into practice at the Advanced Light Source [14], BESSY [15] and the Swiss Light Source [16].

We combine the ultrafast, ultrasmall optical and x-ray pulses using the x-ray microprobe method [17]. Basically, focused laser pulses ( $30 \mu\text{m}$ ) are overlapped in time and space with microfocused x-ray pulses ( $10 \mu\text{m}$ ). Gas-phase systems are particularly suitable for illustrating the basic principles underlying laser control of ultrafast x-ray processes. We discuss two different scenarios for modifying resonant x-ray absorption near an inner-shell edge: (1) modification of electronic structure of inner-shell-excited systems by laser dressing at  $10^{12}$ – $10^{13}$  W/cm<sup>2</sup>; (2) control of resonant x-ray absorption by molecules through laser-induced spatial alignment at  $10^{11}$ – $10^{12}$  W/cm<sup>2</sup>. We also discuss modifications to

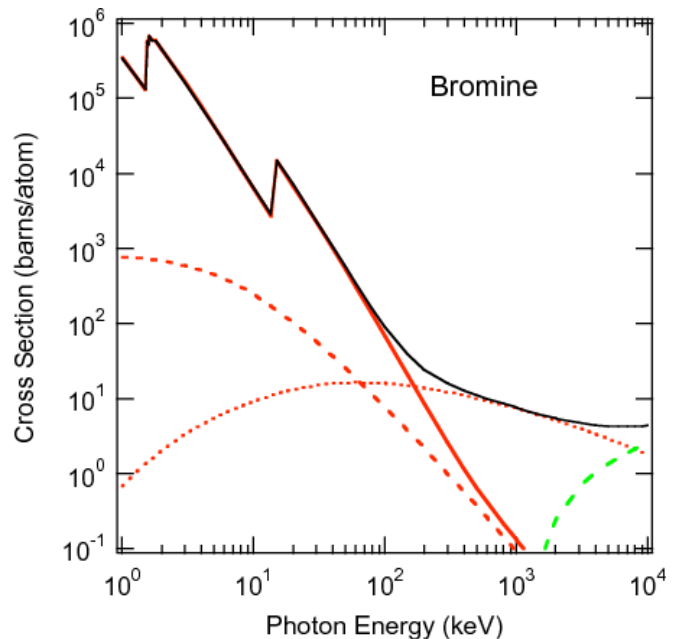


FIG. 2: (Color online) X-ray photoprocesses for bromine. Photoabsorption (solid line) is the dominant process; the  $K$  and  $L$  edges are visible. Rayleigh scattering (dashed line). Compton scattering (dotted line). Synchrotron radiation covers the range from 10 eV to 100,000 eV.

elastic scattering patterns from an ensemble of laser-aligned molecules. Another method to modify resonant x-ray absorption is through strong-field ionization of the target particles at laser intensities in the range  $10^{14}$ – $10^{15}$  W/cm<sup>2</sup> [17, 18, 19]. Fig. 3 illustrates the microprobe and these applications.

Beyond optical laser control of x-ray processes, it is also possible for strong electromagnetic fields at x-ray wavelengths to modify characteristic x-ray processes. The high x-ray intensities required for these modifications will soon be available with x-ray free electron lasers [20, 21, 22].

## CONTROL OF X-RAY PROCESSES WITH STRONG OPTICAL FIELDS

### Electromagnetically induced transparency for x rays: atoms

In this subsection we describe laser-induced modifications to x-ray absorption spectra in various rare gases. Theoretical considerations are described in detail elsewhere [6, 7, 23]. Here we focus on the analogy to electromagnetically induced transparency in the optical regime and the application to imprinting ultrashort optical pulse sequences and shapes onto longer x-ray pulses.

Electromagnetically induced transparency in the optical regime has been widely studied [24, 25, 26]. In a  $\Lambda$ -

# Strong-field control of x-ray processes

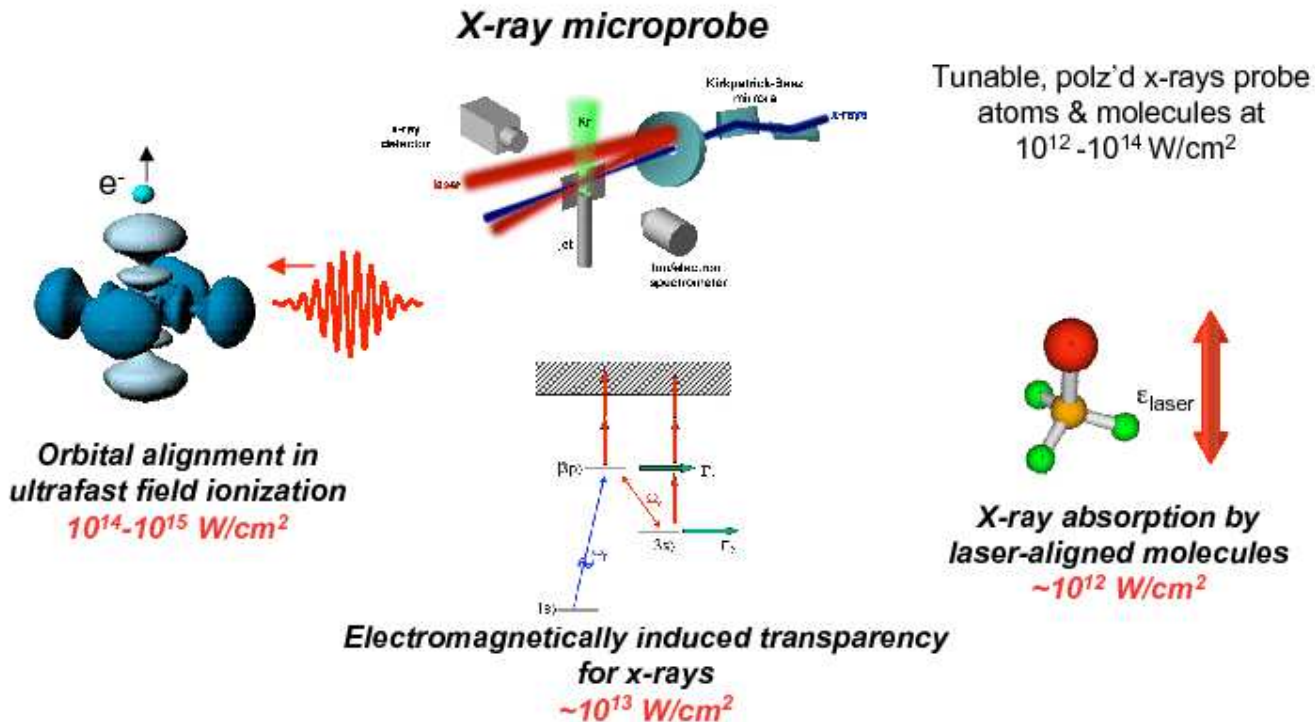


FIG. 3: (Color online) X-ray microprobe and various scenarios for laser control of x-ray absorption at field strengths ranging from  $10^{12} - 10^{15} \text{ W/cm}^2$ .

type medium characterized by atomic levels  $|1\rangle$ ,  $|2\rangle$ , and  $|3\rangle$  with energies  $E_1 < E_2 < E_3$ , resonant absorption on the  $|1\rangle \rightarrow |3\rangle$  transition can be strongly suppressed by simultaneously irradiating the medium with an intense laser that couples the levels  $|2\rangle$  and  $|3\rangle$ . This phenomenon, shown in Fig. 4a, is known as electromagnetically induced transparency, EIT.

In the x-ray regime, EIT is considerably more complex. In the optical regime, levels  $|1\rangle$  and  $|2\rangle$  are stable to electronic decay. However, in the x-ray regime the core-excited states,  $|2\rangle$  and  $|3\rangle$  are metastable. For the three-level system in neon, depicted in Fig. 4b, the lifetime for these core-excited states is 2.4 fs (0.27 eV). Thus, at an optical field strength sufficient to compete with inner-shell decay, multiphoton transitions to the continuum can also play a role. Inner-shell decay rates are denoted by  $\Gamma_2$  and  $\Gamma_3$  and multiphoton transitions to the continuum are denoted by red block arrows.

For the model system in neon, the calculated x-ray photoabsorption cross section for 800 nm laser dressing of the  $1s \rightarrow 3p$  transition in neon at  $10^{13} \text{ W/cm}^2$  with parallel and perpendicular laser/x-ray polarizations along with a fit to a three-level EIT model [7] is reproduced here for convenience in Fig. 5. At this intensity the

$1s \rightarrow 3p$  excitation at 867 eV is suppressed by a factor of 13 for the configuration in which the laser and x-ray polarizations are parallel. As can be seen in Fig. 5, the three level model reproduces most features of the calculated laser-dressed x-ray photoabsorption spectrum. In the three-level model effective linewidths of  $\Gamma_3 = 0.68 \text{ eV}$  and  $\Gamma_2 = 0.54 \text{ eV}$  account for the laser-ionization broadening. These parameters effectively reproduce both the lineshapes for the parallel and perpendicular configurations in the vicinity of the  $1s \rightarrow 3p$  resonance.

The ability to control x-ray absorption in Ne at the  $1s \rightarrow 3p$  resonance allows one to imprint pulses shapes of the optical dressing laser onto long x-ray pulses [7]. This idea is illustrated in Fig. 6. With a 2 mm-long gas cell with one atmosphere of neon, the transmission of an x-ray pulse resonant with the  $1s \rightarrow 3p$  transition will be only 0.07%. A typical x-ray pulse from a synchrotron source has a duration of 100 ps. Such an x-ray pulse may be overlapped in time and space with one or several, ultrashort intense laser pulses. Those portions of the x-ray pulse that overlap with the laser are transmitted through the gas cell. In the case shown in Fig. 6, where the two dressing laser pulses have a peak intensity of  $10^{13} \text{ W/cm}^2$ , the intensity of the two transmitted

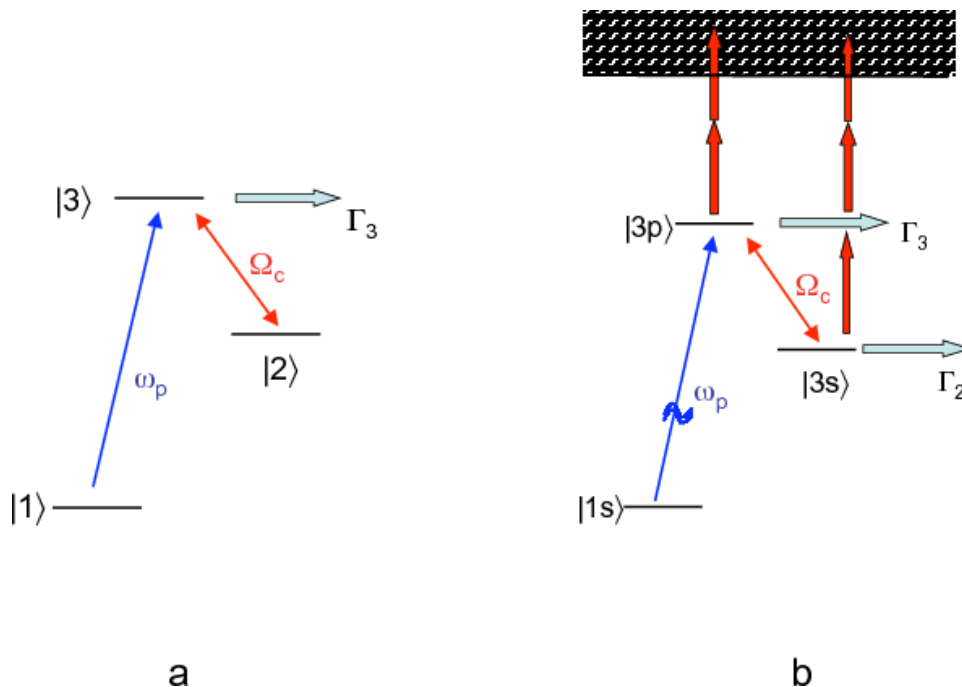


FIG. 4: (Color online) (a) Optical EIT. (b) X-ray EIT in neon.

x-ray pulses is roughly 60% of the incoming pulse. The time delay between the two x-ray pulses can be controlled by changing the time delay between the two laser pulses, opening a route to ultrafast all x-ray pump-probe experiments. With an analogous strategy, controlled shaping of short-wavelength pulses might become a reality. A disadvantage of this method is that it is applicable only at certain x-ray energies; the Ne case operates at 867 eV.

It would be interesting to be able to extend these concepts to the hard x-ray regime. Calculations on the laser-dressed spectra near the  $K$  edge in krypton [6] and argon [27] have been done. In argon and krypton,  $K$  edges are at 3.2 keV and 14.3 keV, respectively. The difficulty is that the inner shell decays are significantly more rapid; for Ne, Ar, Kr the decay widths of core-excited  $1s^{-1}np$  levels are 0.27, 0.6 and 2.7 eV. The increased widths have two consequences. First, the  $1s \rightarrow np$  transitions are not fully resolved as the level width increases, making it difficult to isolate a three-level system. For example, the  $1s^{-1}5p$ ,  $1s^{-1}6p$ , transitions near the krypton  $K$  edge are blended such that it is smooth edge. Second, the laser intensity needed to perturb the x-ray absorption cross section roughly scales as the square of the level width. Thus, when a dressing field of  $10^{13}$  W/cm<sup>2</sup> is applied, the Kr absorption cross section changes by less than 20%.

One possible way to overcome these issues is to use rare gas ions as the EIT medium. The singly ionized krypton atom has a prominent, isolated resonance due to the  $4p$  hole orbital [17, 19, 28]. X-ray absorption spectra for Kr, Kr<sup>1+</sup> and Kr<sup>2+</sup> are shown in Fig. 7. In addition to the isolated resonance, ions can withstand higher

dressing intensities without ionization. The critical field strength,  $E_{crit}$  that one can apply to an atom without ionizing it can be estimated by combining the laser and Coulomb potential,  $E_{crit} = E_{IP}^2 / (4Ze^3)$ , where  $E_{IP}$  is the ionization potential,  $Z$  is the charge of the residual ion,  $e$  is the electron charge [29]. For Kr, Kr<sup>1+</sup> and Kr<sup>2+</sup> the ionization potentials are 14.0, 27.9 and 41.8 eV, respectively. Thus, one should be able to apply a laser intensity  $9 \times$  higher for Kr<sup>2+</sup> than neutral krypton to generate a sizable change in absorption cross section. Of course, generating a sufficient density of ions to realize a practical hard x-ray pulse shaper would be a challenge.

### X-ray absorption and scattering using laser-aligned molecules

In the presence of a strong non-resonant linearly polarized laser field, molecules align due to the interaction of the laser electric field vector with the anisotropic molecular polarizability [5, 30]. The alignment process is of intrinsic interest and of interest in applications to spectroscopy and photophysics, quantum control of molecular dynamics, high-harmonic generation, chemical reactivity, liquids and solvation and structural determinations by x-ray or electron diffraction. For asymmetric molecules having three distinct moments of inertia, 3D alignment has been achieved both in the presence of a laser-aligning field (adiabatic alignment) [31] and under field-free conditions (impulsive alignment) [32]. X-ray probes of laser-aligned molecules are of considerable

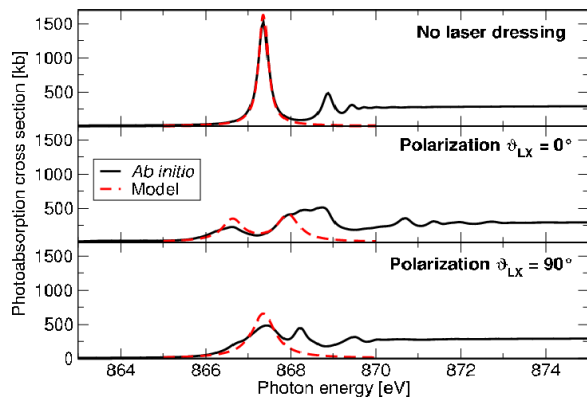


FIG. 5: (Color online) Photoabsorption near the  $1s \rightarrow 3p$  resonance in neon. Results from *ab initio* calculations and a three-level model are shown. From [7].

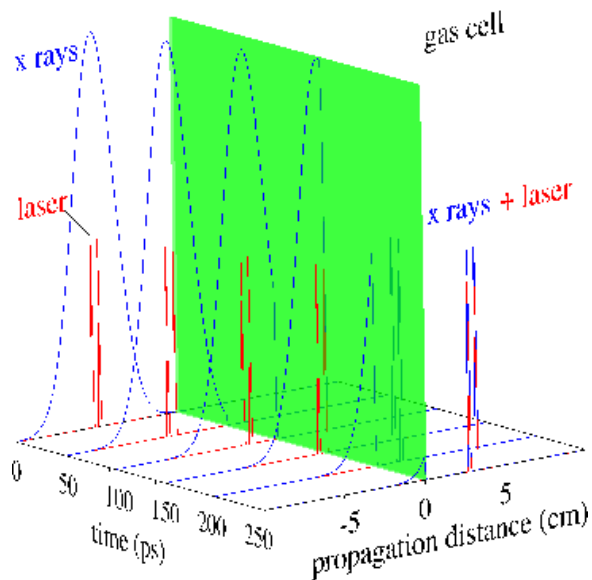


FIG. 6: (Color online) Generation of ultrafast x-ray pulses using laser dressing of Ne. See the text for details.

current interest [8] because of proposals to determine structure of non-periodic specimens, such as individual biomolecules, by x-ray scattering [33, 34] using x-ray free electron lasers.

Both x-ray absorption and scattering from a randomly oriented ensemble of gas phase molecules are significantly modified if the molecules are aligned. In x-ray absorption, both the near-edge and extended structure [extended x-ray absorption fine structure (EXAFS)] can be significantly altered. The near-edge structure is altered when one uses resonant polarized x-ray absorption to detect the alignment of the molecular axis relative to the lab frame [8]. Excitation of a  $1s$  electron to the lowest unoccupied molecular orbital, LUMO, often results in an isolated resonance near the  $K$ -edge of a molecule. The LUMO is fixed relative to the molecular frame and the

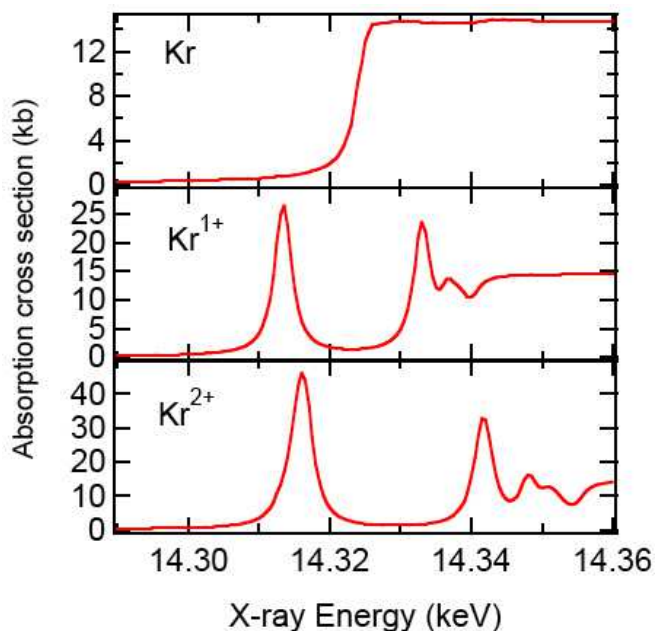


FIG. 7: (Color online) X-ray absorption spectra for Kr,  $\text{Kr}^{1+}$  and  $\text{Kr}^{2+}$ .

transition strength from a highly localized  $K$  shell orbital to the LUMO defines the alignment of the molecule relative to the x-ray polarization axis [35]. For the molecule that we studied,  $\text{CF}_3\text{Br}$ , the LUMO is an antibonding  $\sigma^*$  orbital with substantial  $\text{Br } 4p_z$  character, where  $z$  refers to the C–Br axis. The molecular symmetry dictates that x-ray absorption on the  $\text{Br } 1s \rightarrow \sigma^*$  resonance occurs only when the x-ray polarization vector has a non-vanishing projection on the C–Br axis. Since the laser polarization axis defines the molecular alignment axis, one achieves control of x-ray absorption by simply rotating a waveplate. After aligning in space, time and x-ray energy, i.e., tuning to the  $1s \rightarrow \sigma^*$  resonance at 13.476 keV, the control of resonant x-ray absorption in the near-edge region can be readily achieved [8, 36], as shown in Fig. 8.

In the EXAFS region, modifications to the polarized x-ray absorption will also be induced by molecular alignment. Pictorially, the effect for  $\text{Br}_2$  is shown in Fig. 9. When the  $\text{Br}_2$  molecules are aligned parallel to the x-ray polarization axis, the modulation of the absorption cross section due to  $\text{Br } 1s \rightarrow \epsilon p$  photoelectron backscattering from the adjacent atom is maximal, and in a perpendicular configuration minimal. Thus, the magnitude of the EXAFS modulation is controlled by the angle of the molecular axis relative to the x-ray polarization axis. The equation describing the modulation around an atomic background is given by

$$\chi(k) = - \sum_i \frac{3 \cos^2 \vartheta_i}{k R_i^2} F_i(k) e^{-2\sigma_i k^2} e^{-2R_i/\lambda_i(k)} \times \sin(2kR_i + 2\delta_l + \beta_i), \quad (1)$$

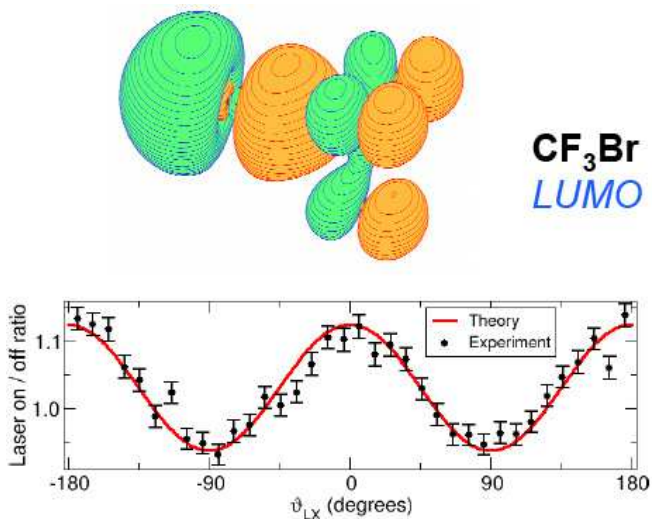


FIG. 8: The LUMO of CF<sub>3</sub>Br is an antibonding  $\sigma^*$  orbital with substantial Br 4p<sub>z</sub> character, where  $z$  refers to the C–Br axis. X-ray absorption on the  $1s \rightarrow \sigma^*$  resonance as a function of the angle between the polarization axis of the aligning laser and that of the x-ray probe.

where  $k$  is the photoelectron wavevector,  $\vartheta_i$  is the angle between the x-ray polarization and the  $i^{\text{th}}$  atom,  $R_i$  is the distance between the central and  $i^{\text{th}}$  atom,  $\sigma_i$  is the Debye-Waller factor,  $\Lambda_i$  is the range parameter for photoelectron scattering and  $\delta_i$  and  $\beta_i$  describe the outgoing photoelectron phase shift [35]. Polarized EXAFS measurements on laser-aligned molecules will permit one to determine changes in structure due to e.g. laser aligning fields, though the utility of EXAFS for absolute bond distances may be limited. Laser control of the angle between the molecular and x-ray polarization axes will permit control of the EXAFS modulation amplitude, determination of the atomic background and, for more complex molecules, the determination of bond angles.

Elastic scattering will also be modified since the contributions from the aligned molecules can be summed linearly and a scattering pattern reflective of the molecular structure will emerge. A simulation of the x-ray scattering pattern from an ensemble of molecules aligned by a laser pulse of arbitrary shape was made. First the molecular response to the laser pulse was calculated [36] and then the x-ray scattering [37] from this ensemble was simulated. In Fig. 10 elastic scattering patterns for an isotropic sample, for clamped nuclei and for an alignment of  $\langle \cos^2 \theta \rangle(t) = 0.80$  are shown. As the standard method for absolute molecular structure determination, x-ray diffraction from laser-aligned molecules will then allow us to investigate changes in molecular structure in the presence of strong laser aligning fields with the eventual goal of a predictive understanding using an *ab initio* electronic structure code such as DALTON to calculate molecular hyperpolarizabilities.

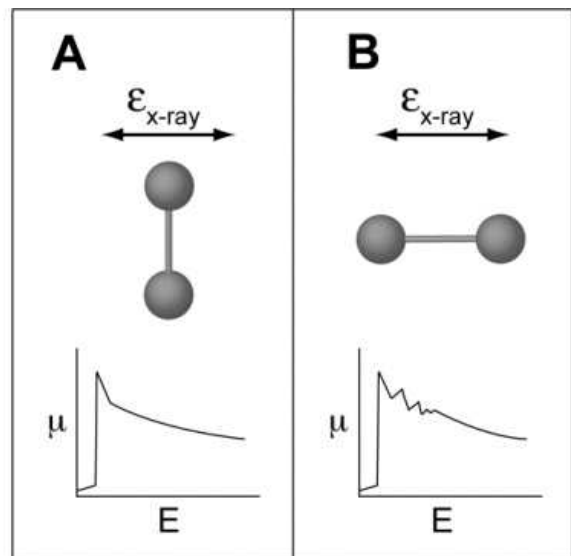


FIG. 9: Schematic of the polarization dependence of the EXAFS modulations in Br<sub>2</sub>.

#### MODIFYING CHARACTERISTIC X-RAY PROCESSES WITH STRONG X-RAY FIELDS

In the previous section we have seen how it is possible to control resonant x-ray absorption with optical fields. With focused x-ray free electron lasers it will be possible to create intensities such that characteristic x-ray processes are altered. A simple estimate may be made for the  $1s \rightarrow 3p$  transition in neon. Here the transition dipole matrix element is  $0.01ea_0$  [38] rather than the  $1.05ea_0$  for the hydrogen  $1s \rightarrow 2p_{1/2}$  transition. Equating the Rabi frequency with the core-excited decay rate  $(2.4 \text{ fs})^{-1}$  suggests that an intensity of  $10^{18} \text{ W/cm}^2$  is required to saturate this transition. Focusing the LCLS output at 800 eV ( $10^{13}$  photons / 233 fs) to a spot size of  $\sim 1 \mu\text{m}$  will yield this intensity. At high intensity, the ejection of a second electron from the  $1s$  shell can be more rapid than Auger decay to create hollow neon, Ne[KK] [39]. The intensity dependence is shown in Fig. 11. As one can see, hollow neon is formed preferentially at higher intensity; indeed Ne[KK] can be the dominant species, compared to the usual 1% fraction in the weak field limit. Because the LCLS output originates from SASE (self-amplified spontaneous emission), the output radiation is chaotic, consisting of a random number of intensity spikes (coherent regions) of random amplitude. Therefore, one might expect an enhancement of two-photon processes (such as Ne[KK] formation). In the lower part of Fig. 11, the Auger yield from an ensemble average of chaotic pulses is compared with the yield from an average pulse shape. As one can see, the chaotic enhancement for Ne[KK] production is at most a factor of 1.3 in the unsaturated regime. This is in contrast to visible radiation where one expects

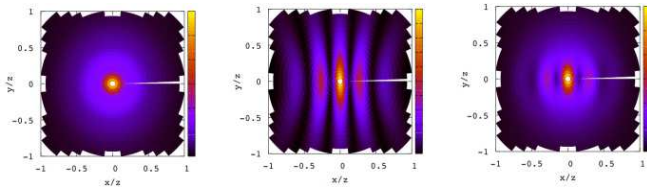


FIG. 10: Elastic scattering from isotropic, fixed-in-space and aligned  $\text{Br}_2$  with  $\langle \cos^2 \theta \rangle > (t) = 0.80$ .

a factor of 2. The critical quantity is the ratio of the FEL coherence time to the Auger lifetime. The larger the ratio, the closer one will be to the maximal enhancement of 2. Finally, we note that fully stripped neon can be produced in the  $1 \mu\text{m}$  focus of the LCLS beam by sequential single photon processes, providing the photon energy is greater than the binding energy of  $\text{Ne}^{9+}$  [39].

## OUTLOOK

The era in which characteristic x-ray processes can be considered invariant is at an end. We have demonstrated that placing atoms and molecules in strong optical fields can significantly affect resonant absorption and elastic scattering. Currently, we can control x-ray absorption with application of a strong-optical field to a gaseous medium; the control mechanism is EIT in atoms and laser-constrained rotation in molecules. One may be able to create an x-ray amplitude pulse shaper using these tools. X-ray scattering from aligned molecules is not far off; simple estimates show that a mere  $10^8$  x-rays/pulse at 1 kHz will suffice as obtainable with a pink beam at the Advanced Photon Source [8]. In addition, we look forward to being able to experimentally observe multiphoton processes in the hard x-ray regime when LCLS is first operational in 2009. Control of molecular alignment combined with subsequent ion/electron imaging techniques will provide a means to disentangling x-ray damage mechanisms in complex molecules.

We thank Dohn A. Arms, Eric M. Dufresne, Eric C. Landahl, and D. Walko for valuable assistance during experiments at the Sector 7 beamline at the Advanced Photon Source. C.B. was partly supported by a Feodor Lynen Research Fellowship from the Alexander von Humboldt Foundation. This work and the Advanced Photon Source were supported by the Chemical Sciences, Geosciences, and Biosciences Division of the Office of Basic Energy Sciences, Office of Science, U.S. Department of Energy, under Contract No. DE-AC02-06CH11357.

\* Present address: Department of Physics and Astronomy, Louisiana State University, Baton Rouge,

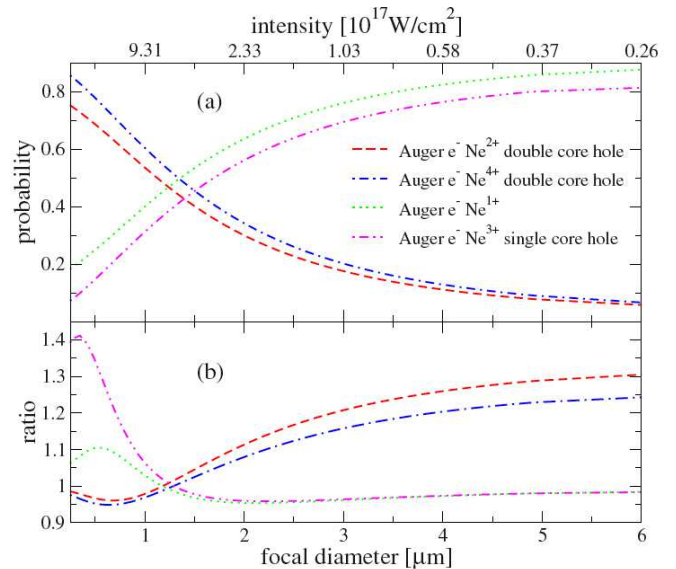


FIG. 11: (Color online) Top: Yield of  $\text{Ne}[\text{K}]$  and  $\text{Ne}[\text{KK}]$  as a function of focused LCLS intensity at a photon energy of 1050 eV. Bottom: Ratio of Auger yields from an ensemble average of chaotic SASE pulses to that from an averaged pulse. From [39].

Louisiana 70803, USA

† Present address: Lawrence Livermore National Laboratory, Livermore, California 94551, USA

- [1] R. Santra, R. W. Dunford, E. P. Kanter, B. Krässig, L. Young, “Strong Field Control of X-ray Processes” in *Advances in Atomic, Molecular and Optical Physics*, Volume 56, (Elsevier, Amsterdam, Netherlands, 2008).
- [2] S. A. Rice, M. Zhao, *Optical Control of Molecular Dynamics*, (Wiley, New York, 2000).
- [3] M. Shapiro, P. Brumer, *Principles of the Quantum Control of Molecular Processes*, (Wiley-Interscience, New York, 2003).
- [4] H. Rabitz, R. de Vivie-Riedle, M. Motzkus, K. Kompa, *Science* **288**, 824 (2000).
- [5] H. Stapelfeldt, T. Seideman, *Rev. Mod. Phys.* **75**, 543 (2003).
- [6] C. Buth, R. Santra, *Phys. Rev. A* **75**, 033412 (2007).
- [7] C. Buth, R. Santra, L. Young, *Phys. Rev. Lett.* **98**, 253001 (2007).
- [8] E. R. Peterson, C. Buth, D. A. Arms, R. W. Dunford, E. P. Kanter, B. Krässig, E. C. Landahl, S. T. Pratt, R. Santra, S. H. Southworth, L. Young, *Appl. Phys. Lett.* **92**, 094106 (2008).
- [9] M. O. Krause, *J. Phys. Chem. Ref. Data* **8**, 307 (1979).
- [10] T. Brabec, F. Krausz, *Rev. Mod. Phys.* **72**, 545 (2000).
- [11] G. A. Mourou, T. Tajima, S. V. Bulanov, *Rev. Mod. Phys.* **78**, 309 (2006).
- [12] D. Strickland, G. Mourou, *Opt. Commun.* **56**, 219 (1985).
- [13] A. A. Zholents and M. S. Zolotarev, *Phys. Rev. Lett.* **76**, 912 (1995).
- [14] R. W. Schoenlein, S. Chattopadhyay, H. H. W. Chong, T. E. Glover, P. A. Heimann, C. V. Shank, A. A. Zholents, M. S. Zolotarev, *Science* **287**, 2237 (2000).
- [15] S. Khan, K. Holldack, T. Kachel, R. Mitzner, and T. Quast, *Phys. Rev. Lett.* **97**, 074801 (2006).

- [16] P. Beaud, S. L. Johnson, A. Streun, R. Abela, D. Abramsohn, D. Grolimund, F. Krasniqi, T. Schmidt, V. Schlott, and G. Ingold, *Phys. Rev. Lett.* **99**, 174801 (2007).
- [17] L. Young, D. A. Arms, E. M. Dufresne, R. W. Dunford, D. L. Ederer, C. Höhr, E. P. Kanter, B. Krässig, E. C. Landahl, E. R. Peterson, J. Rudati, R. Santra, S. H. Southworth, *Phys. Rev. Lett.* **97**, 083601 (2006).
- [18] R. Santra, R. W. Dunford, L. Young, *Phys. Rev. A* **74**, 043403 (2006).
- [19] S. H. Southworth, D. A. Arms, E. M. Dufresne, R. W. Dunford, D. L. Ederer, C. Höhr, E. P. Kanter, B. Krässig, E. C. Landahl, E. R. Peterson, J. Rudati, R. Santra, D. A. Walko, L. Young, *Phys. Rev. A* **76**, 043421 (2007).
- [20] J. Arthur *et al.*, *Linac Coherent Light Source (LCLS) Conceptual Design Report*, SLAC-R-593, 2002.
- [21] T. Tanaka and T. Shintake, *SCSS X-FEL Conceptual Design Report*, RIKEN Harima Institute/SPring-8, 2005.
- [22] M. Altarelli *et al.*, *The Technical Design Report of the European XFEL*, DESY 2006-097, 2006.
- [23] C. Buth, R. Santra, and L. Young, in this proceedings.
- [24] S. E. Harris, J. E. Field, and A. Imamoglu, *Phys. Rev. Lett.* **64**, 1107 (1990).
- [25] K. J. Boller, A. Imamoglu, and S. E. Harris, *Phys. Rev. Lett.* **66**, 2593 (1991).
- [26] S. E. Harris, *Phys. Today* **50**, No. 7, 36 (1997).
- [27] C. Buth and R. Santra, to be published.
- [28] L. Pan, D. R. Beck, S. M. O'Malley, *J. Phys. B.* **38**, 3721 (2005).
- [29] S. Augst, D. Strickland, D. D. Meyerhofer, S. L. Chin, J. H. Eberly, *Phys. Rev. Lett.* **63**, 2212 (1989).
- [30] B. Friedrich and D. Herschbach, *Phys. Rev. Lett.* **74**, 4623 (1995).
- [31] J. J. Larsen, K. Held, N. Bjerre, H. Stapelfeldt, and T. Seideman, *Phys. Rev. Lett.* **85**, 2470 (2000).
- [32] K. F. Lee, D. M. Villeneuve, P. B. Corkum, A. Stolow, and J. G. Underwood, *Phys. Rev. Lett.* **97**, 173001 (2006).
- [33] R. Neutze, R. Wouts, D. van der Spoel, E. Weckert, and J. Hajdu, *Nature* **406**, 752 (2000).
- [34] J. C. H. Spence and R. B. Doak, *Phys. Rev. Lett.* **92**, 198102 (2004).
- [35] J. Stöhr, *NEXAFS Spectroscopy* (Springer, New York, 1996).
- [36] C. Buth and R. Santra, *Phys. Rev. A* **77**, 013413 (2008).
- [37] P. Ho and R. Santra, to be published.
- [38] N. Rohringer and R. Santra, *Phys. Rev. A* (in press).
- [39] N. Rohringer and R. Santra, *Phys. Rev. A* **76**, 033416 (2007).